Capture and release of tRNA by the T-loop receptor in the function of the T-box riboswitch

Xianyang Fang[a,b], Malgorzata Michnicka[c] , Yikan Zhang [a],Yun-Xing Wang[b] and Edward P. Nikonowicz[c,*]

[a]Beijing Advanced Innovation Center for Structural Biology, School of Life Sciences, Tsinghua University, Beijing, China,100084;

[b]Structural Biophysics Laboratory, National Cancer Institute, Frederick, MD 21702;

[c]Department of BioSciences, Rice University, Houston, TX 77005.

* To whom correspondence should be addressed. Tel: 713-348-4912; Fax: 713-348-5154; Email: edn@rice.edu

Correspondence may also be addressed to Xianyang Fang. Email: fangxy@tsinghua.edu.cn

Key words

SAXS, heteronuclear NMR, tRNA, transcription regulation, riboswitch, anti-termination

Abbreviations

SAXS, small-angle X-ray scattering; HSQC, heteronuclear single quantum coherence; ITC, isothermal titration calorimetry; SEC, size exclusion chromatography.

Abstract

In Gram-positive bacteria, the tRNA-dependent T-box riboswitch system regulates expression of amino acid biosynthetic and aminoacyl-tRNA synthetase genes through a transcription attenuation mechanism. Binding of uncharged tRNA “closes” the switch, allowing transcription read-through. Structure studies of the 100 nt stem I domain reveal tRNA utilizes base pairing and stacking interactions to bind the stem, but little is known structurally about the 180 nt riboswitch core (stem I, stem III, and antiterminator stem) in complex with tRNA and the mechanism of coupling of the intermolecular binding domains crucial to T-box function. Here we utilize solution structural and biophysical methods to characterize the interplay of the different riboswitch-tRNA contact points using *B. subtilis* and *O. iheyensis* glycyl T-box and T-box:tRNA constructs. The data reveal that tRNA:riboswitch core binding at equilibrium involves only Specifier-anticodon and anti-terminator-acceptor stem pairing. The elbow:platform stacking interaction observed in studies of the T-box stem I domain is released after pairing between the acceptor stem and the bulge in the anti-terminator helix. The results are consistent with the model of T-box riboswitch:tRNA function in which tRNA is captured by Stem I of the nascent mRNA followed by stabilization of the antiterminator helix and the paused transcription complex.

INTRODUCTION

tRNA-mediated transcription attenuation is the primary mechanism of regulation for genes encoding aminoacyl-tRNA (aa-tRNA) synthetases and amino acid biosynthetic enzymes in Gram-positive bacteria and is designated the T-box mechanism [1, 2]. This mechanism employs an intrinsic terminator that destabilizes RNA polymerase and causes release of the DNA template thereby attenuating transcription. The 5' untranslated (or mRNA leader) regions of genes controlled by this mechanism are 200-300 nt in length and function as “riboswitches” that recognize and capture cognate tRNA molecules [2-4]. Binding of uncharged tRNA to the T-box riboswitch is necessary to prevent premature transcription termination. Thus, the T-box riboswitch senses the aminoacylation state of individual tRNA species in the cell and up-regulates gene expression as needed.

All T-box riboswitches contain a core set of secondary structure elements and conserved sequence features that support gene-specific selection of cognate tRNA [4-7]. Stem I contains multiple functionally important structure motifs, including the guanine-adenine (GA) or K-turn motif [8], a loop E motif within the Specifier domain [9-11], and distally positioned T-loop motifs [12, 13]. The loop E motif facilitates presentation of the Specifier sequence, three nucleotides that are complementary to the tRNA anticodon and confer specificity to the T-box-tRNA interaction. Nucleotides near the 3' end of the riboswitch adopt one of two mutually exclusive stem-loop secondary structures designated the terminator and anti-terminator helices. In the anti-terminator helix, four residues of a seven nucleotide bulge (T-box loop) base pair with the terminal 5'-NCCA nucleotides at the 3' end of the tRNA. Although the terminator helix is thermodynamically more stable than the anti-terminator helix, pairing of the T-box loop nucleotides with tRNA stabilizes of the structure and allows read-through of the transcription pause site.

To date, atomic resolution structures have only been determined for several fragments of the T-box riboswitch, including the Specifier domain, K-turn region, and anti-terminator helix by NMR [11, 14, 15], and the complete stem I free and in complex with cognate tRNA by X-ray crystallography [13, 16].

However, little is known about the full-length structure of the T-box riboswitch-tRNA complex. More importantly, almost nothing is known about the interplay between the stem I and anti-terminator binding sites that is crucial to understand the T-box regulatory role. Here we have used small angle x-ray scattering (SAXS) and NMR spectroscopy to develop topological structural models of the anti-terminator state of a glycyl T-box riboswitch from *Bacillus subtilis* and the riboswitch-tRNA complex. Our data support a mechanistic model in which tRNA is captured by stem I via the Specifier sequence-anticodon and T-loop platform-tRNA elbow interactions followed by pairing of the T-box loop with the 3' terminus of the tRNA [17] and release of the tRNA elbow. Furthermore, we show that a loss-of-function point mutation in the apical loop prevents formation of a stable double T-loop motif involving the terminal loop of stem I [10]. Lastly, we demonstrate that nucleotide substitution $C_{32}U$ in $tRNA_2^{Gly}$, modified to include anticodon 5'-GCC-3', decreases affinity of the tRNA for stem I by 8-fold.

MATERIALS AND METHODS

Sample preparation. The RNA molecules were prepared by in vitro transcription with T7 RNA polymerase. DNA templates were generated by PCR from gBlocks Gene Fragments (Integrated DNA Technologies) and the PCR products sequenced prior to use in the transcription reactions. The nucleotide sequence for the T-box riboswitches were derived from the mRNA leader regions of the *B. subtilis glyQS* gene and *Oceanobacillus iheyensis glyQ* gene. Figure 1A shows the native riboswitch molecule (180 nt) that is composed of stem I, stem III, and the antiterminator stem and Figure 2 shows four riboswitch variants: *i-stem I* has an 18 bp helix inserted into stem I, *i-stem III* has an 18 bp helix inserted into stem III, *i-stem AT* has an 18 bp helix inserted into the antiterminator stem, and *short-stem I* in which the apical loop of stem I has been deleted. Riboswitch RNA molecules were purified using 16% (w/v) non-denaturing, preparative polyacrylamide gels, electroeluted, and dialyzed 1:10,000 against buffer A (150 mM KCl, 15 mM MOPS (pH 6.8), 2.0 mM DTT, 0.5% glycerol, and 17 mM $MgCl_2$). Some duplicate samples were prepared using 3 mM $MgCl_2$. tRNA molecules were purified using 20% (w/v) denaturing polyacrylamide gels, electro-eluted, and precipitated from ethanol. The purified tRNA molecules were suspended in 1.0 M KCl, 20 mMKPi, pH 6.8 and 0.02 mM EDTA and extensively

dialyzed against 150 mM KCl, 15 mM MOPS (pH 6.8), and 0.02 mM EDTA. tRNA molecules were annealed twice by heating to 90 °C for 1 minute and snap cooled on ice. The samples were brought to 17 mM $MgCl_2$ and 0.5% glycerol and annealed again by heating to 45 °C and slowly (30 minutes)

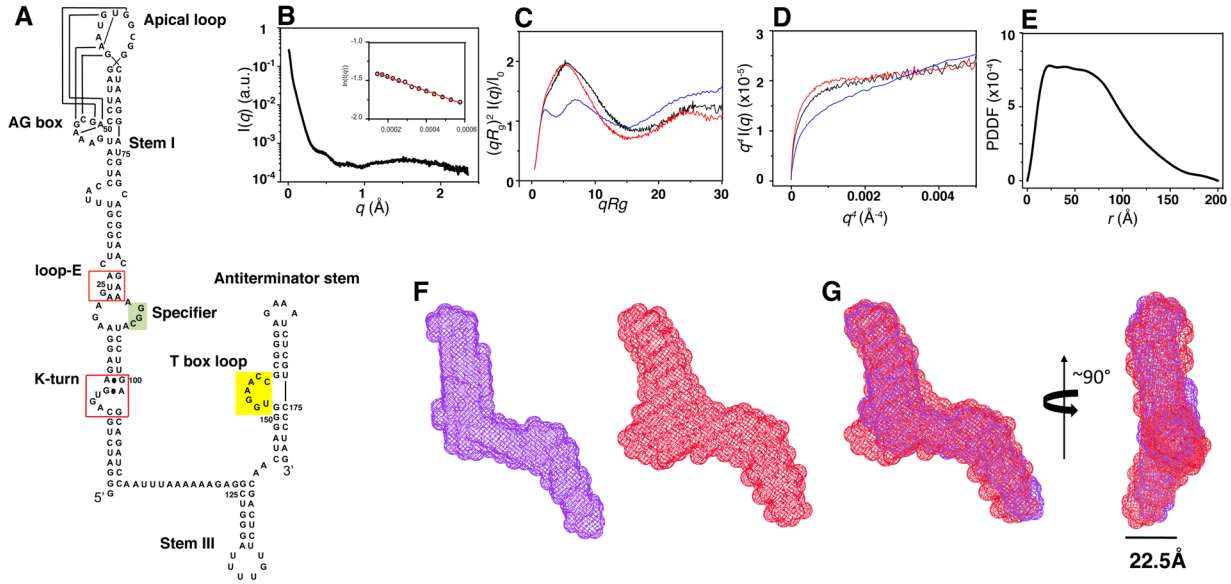

Figure 1. (A) Secondary structure of the T-box riboswitch core molecule. This form of the T-box riboswitch is designed to model the configuration of the anti-termination state. The Specifier sequence in stem I is highlighted in green and nucleotides of the T-box loop are highlighted in yellow. (B) Plot of SAXS scattering intensity in arbitrary units versus momentum transfer q in $Å^{-1}$. The Guinier region (*inset*) is linear indicating the sample is monodisperse. The dimensionless Kratky plots (C) and the Porod-Debye plots (D), tend asymptotically to constant values for T-box riboswitch core (black) and its tRNA complex (red) indicating that the RNA and its tRNA complex are well folded particles and contain no long disordered regions. The similar plots for the HIV-1 rev response element (RRE) RNA were included for comparison, indicating T-box core and its complex are no more flexible or extended than RRE. (E) The pair distance distribution function of the riboswitch core molecule calculated using GNOM (q_{max}=0.3). (F) The molecular envelope of the riboswitch core molecule at 3mM Mg^{2+} (blue) and 17 mM Mg^{2+} (red). (G) The molecular envelope of the riboswitch core molecule at 3mM Mg^{2+} was superimposed onto that at 17 mM Mg^{2+}.

cooling to 20°C twice. Complexes were prepared by mixing riboswitch core molecules with 10% stoichiometric excess of tRNA followed by centrifugation dialysis against buffer A using 50 kDa cutoff filter membranes (to remove excess tRNA and the flow-through checked for A_{260} absorbance) and the complexes confirmed on native gel. Three riboswitch constructs (native, i-stem III, and i-stem AT, containing the bacterial ribosomal protein S8 binding site at the 3' ends were also prepared as a control for riboswitch folding and SAXS envelope quality. His_6-tagged S8 protein from *Escherichia coli* (over-expressed from a pET-28b vector and purified in house) was used to isolate full-length T-box riboswitch molecules from the transcription reaction and the S8-riboswitch complexes captured using Ni^{2+} resin and washed with 150 mM KCl, 15 mM MOPS (pH 6.8), 10 mM $MgCl_2$, 0.5% glycerol, and 5

mM imidazole to remove free RNA molecules. S8-riboswitch complexes were released from the resin by washing with 100 mM imidazole and dialyzed against buffer A. T-box riboswitch and tRNA concentrations were ~0.085 mM and ~0.25 mM, respectively. The final RNA concentrations in the SAXS samples were 0.025 – 0.055 mM. The ^{15}N-labeled RNA molecules used in the NMR experiments were prepared as described [18]. The PAGE purified RNA molecules were dialyzed extensively against 10 mM KCl, 5 mM sodium potassium phosphate (pH 6.8), and 0.02 mM EDTA and lyophilized. The RNA samples were suspended in 0.35 ml of 99.96% D_2O or 90% H_2O/10% D_2O and annealed and contained 50-150 A_{260} OD units of RNA oligonucleotide (≈0.25–0.8mM).

NMR spectroscopy. All NMR spectra were acquired on Varian Inova 600 and 800 MHz spectrometers equipped with cryogenically cooled ^{1}H–[^{13}C, ^{15}N] probes and solvent suppression was achieved using binomial read pulses. 2D ^{15}N-^{1}H HSQC spectra were collected to identify ^{15}N-^{1}H chemical shift correlations. 2D NOESY and NOESY-HSQC spectra (τ_{mix} =300 ms) and were acquired at 16 °C to obtain sequence specific NH ^{1}H resonance assignments. Typically, the data points were extended by 25% using linear prediction for the indirectly detected dimensions. NMR spectra were processed and analyzed using Felix 2007 (Felix NMR Inc., San Diego, CA).

Isothermal titration calorimetry. A titration calorimeter (MicroCal, Inc.) was used for the ITC experiments. RNA molecules corresponding stem I of the *B. subtilis glyQS* and *O. ilheyensis glyQ* riboswitches and the *B. subtilis* $tRNA_2^{Gly,gcc}$ and its C32U variant were synthesized using T7 RNA polymerase as described above. RNA samples were extensively dialyzed against buffer A. The concentrations of RNA in the injection syringe and sample cell were 0.270 mM (tRNA) and 0.022 mM (stem I), respectively. For the titration experiments, 30 10 μL injections into 1.5 mL sample cell volume were performed with 5 minutes between injections. The sample was stirred constantly at 290 rpm and the temperature was set to 12 °C. The ITC data were analyzed using the vendor-supplied software (ORIGIN v7.0) and plots of ΔH versus mole ratio were generated from the raw thermograms. The final 3-5 points from each experiment were extrapolated to obtain a straight line that was subtracted from

all the data before determining ΔH, (the overall reaction enthalpy), K_A (association constant), and n (reaction stoichiometry) by fitting the points using a non-liner least squares model for a single binding site.

Small angle X-ray scattering. X-ray scattering measurements were carried out at room temperature at the beamlines 12ID-B &-C of the Advanced Photon Source, at the Argonne National Laboratory. The setups were adjusted to achieve scattering q values of $0.006 < q < 2.3 Å^{-1}$ (12ID-C) or $0.005 < q < 2.8 Å^{-1}$ (12ID-B), where $q = (4\pi/\lambda)\sin\theta$, and 2θ is the scattering angle. Twenty 2-dimensional images were recorded for each buffer or sample solution using a flow cell, with the exposure time of 0.5-2 seconds to minimize radiation damage and obtain good signal-to-noise ratio. No radiation damage was observed as confirmed by the absence of systematic signal changes in sequentially collected X-ray scattering images and also confirmed later by gel electrophoresis. The 2D images were reduced to one-dimensional scattering profiles using Matlab. Scattering profiles of the RNAs were calculated by subtracting the background buffer contribution from the sample-buffer profile. The experimental radius of gyration (R_g) was calculated from data at low q values in the range of $qR_g < 1.3$, using the guinier approximation of $\ln I(q) \approx \ln(I(0)) - R_g^2 q^2/3$. The pair distance distribution function (PDDF), $p(r)$, and the maximum dimension of the protein, D_{max}, in real space was calculated with the indirect Fourier transform program GNOM [19]. To avoid underestimation of the molecular dimension and consequent distortion in low resolution structural reconstruction, the parameter D_{max} (the upper end of distance r), was chosen so that the resulting pair distance distribution function (PDDF) has a short, near zero-value tail. Low resolution ab initio shape reconstructions were performed with the programs DAMMIN or DAMMIF, which generate models represented by an ensemble of densely packed beads [19], using scattering data within the q range of 0.007 -0.30 $Å^{-1}$. 32 independent runs for both programs were performed, and the resulting models were subjected to averaging by DAMAVER [20] and were superimposed by SUPCOMB [21] based on the normalized spatial discrepancy (NSD) criteria and were filtered using DAMFILT to generate the final model.

Three-dimensional modeling of the T-box riboswitch. Beginning with the secondary structure of *B.*

subtilis glyQS T-box riboswitch, the distal end of stem I was modeled with ModeRNA using the crystal structure of stem I of the *O. iheyensis* T-box riboswitch (PDB: 4lck) as a template. Stem III and the anti-terminator stem of the riboswitch were modeled using RNAComposer. The spatial positioning of the respective domains was guided by the assignments of the SAXS envelope, and the linking residues were added using Xplor-NIH. The resulting models were further subjected to energy minimization using Xplor-NIH.

RESULTS

Solution topological structure of the T-box riboswitch core by SAXS

The sequence and secondary structure of the T-box riboswitch core (Figure 1A) is based on the leader region of the *Bacillus subtilis glyQS* mRNA (Figure S1) and is designed to form only stems I and III and the anti-terminator stem. We refer to this collection of elements as the T-box riboswitch core. This sequence was designed to yield a homogeneous riboswitch population by removing the nucleotide sequence that codes for the thermodynamically more favorable terminator stem-loop and competes with formation of the anti-terminator helix (Figure S1). The overall secondary structure of the T-box riboswitch core is consistent with biochemical and genetic studies [10, 22, 23]. Crystal and solution NMR structures for stem I and the anti-terminator stem confirm the alignment-derived secondary structure and revealed the presence of loop E and double T-loop tertiary structure motifs in stem I [11, 13-16].

We analyzed the three-dimensional topological structure of the T-box riboswitch core using small angle X-ray scattering (SAXS). Figure 1B shows the experimental SAXS profile of the core molecule. The scattering intensity I(q) was measured as a function of the momentum transfer q (Figure 1B). Direct analysis of the data provides additional sample quality control and information about the degree of compactness of the particle. The Guinier region of the scattering profile (inset in Figure 1B) is linear, indicating the sample is monodisperse and homogeneous. The dimensionless Kratky plot (Figure 1C, in black), $(qR_g)^2I(q)/I(0)$versus qR_g, is bell shaped and the Porod-Debye plot [24] (Figure 1D, in black), $I(q)\cdot q^4$ versus q^4, tend asymptotically to a constant value, indicating that the RNA is a well folded particle and contains no long disordered region. Finally, the pair distance distribution

function (PDDF) (Figure 1E), obtained by Fourier transformation of the SAXS profile, is asymmetric with the most populated distance shorter than half of the maximum distance within the molecule (D_{max}), indicating the relative elongated nature of the molecule.

The shape of the T-box riboswitch core was reconstructed by ab initio modeling with DAMMIN and auxiliary programs [19, 25]. This strategy models a macromolecule as an assembly of scattering beads arranged in space such that a calculated scattering curve reproduces the experimental curve and has been employed to determine the shapes of large structured RNAs [26-29]. The resulting average envelope is shown in Figure 1F and demonstrates that the T-box riboswitch core adopts an elongated structure which is not affected by Mg^{2+} concentration. Indeed, the overall topology remains similar at 3 mM and 17 mM of Mg^{2+} concentrations (Figure 1F,G).

Locations of domains in the T-box riboswitch core

To determine the locations of the individual domains of the T-box riboswitch core within the SAXS envelope, we analyzed several riboswitch variants and the overall structural parameters are listed in Table S1. Two variants were generated that shortened (short-stem I) or extended (i-stem I) the length

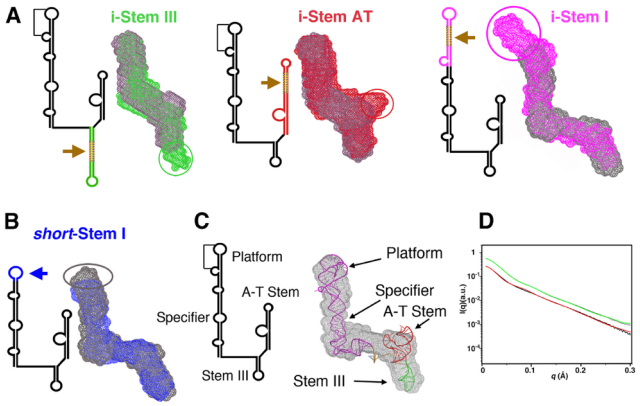

Figure 2. (A) Secondary structure diagrams and molecular envelopes of the three 18 bp stem insertion variants of the riboswitch core: Stem III (green), anti-terminator (A-T) Stem (red), Stem I (pink). The 18 base pair helix (dashed) was inserted into the three riboswitch stems (arrows) to identify stem locations in the SAXS envelope. (B) Secondary structure diagram and molecular envelope of a variant in which stem I was truncated above the AG box (blue). (C) The atomic model of riboswitch core in ribbon superimposed with the SAXS envelope in gray mesh. (D) Comparison of the scattering curves of the experimental data of the riboswitch core (black) and riboswitch core:tRNA complex (gray) to those calculated for the atomic models of the riboswitch core (red) and the complex (green).

of stem I by removing the apical loop or by inserting an 18 base pair helix at the base of the apical loop, respectively (Figure 2A,B and S2A). Comparing the shape of the i-stem I variant with that of the T-box riboswitch core, the extra mass corresponding to the inserted helix is clearly evident (Figure 2A

and S2A). Similarly, substitution of the apical loop with the tetraloop results in modest shortening along one axis of the SAXS envelope (Figure 2B and S2A). The effect of this substitution is consistent with the crystal structure of this region which shows nucleotides in the apical loop fold over to form multiple tertiary interactions with nucleotides in the proximal AG box [12, 13, 16], resulting in similar lengths for native and truncated stems I. Stem III and the anti-terminator stem were identified using variants i-stem III and i-stem AT that were generated by inserting the same 18base pair RNA sequence into the respective helices (Figure 2A and S2B,C). The domains of the T-box riboswitch core were then mapped onto the riboswitch core and an atomic model for the T-box riboswitch core built up and fitted into the SAXS envelope (Figure 2C).

tRNA binding to the T-box riboswitch core

Binding of tRNA to the isolated stem I of the T-box riboswitch includes anticodon-Specifier codon base pairing and stacking of the tRNA elbow against a platform created by nucleotides of the apical loop and AG box [12, 13, 16]. To determine how tRNA is accommodated by the T-box riboswitch core, tRNA-riboswitch complexes were examined using SAXS. A $U_{34}G$ variant of glycyl $tRNA_2$ (anticodon 5'-GCC-3', $tRNA_2^{Gly,gcc}$) (Figure 3A) was prepared by in vitro transcription and therefore does not contain the nucleotide base modifications normally present in the D- and T-loops and anticodon arm. The secondary and tertiary structures of tRNA were used with SAXS data to analyze the three-dimensional structures of the tRNA-riboswitch complexes. The dimensionless Kratky plot (Figure 1C, in red) shows an elevated baseline at smaller qRg and the Porod-Debye plot (Figure 1D, in red) shows a plateau at lower q for the tRNA-riboswitch complex, indicative of decreased flexibility of the riboswitch core upon tRNA binding. The SAXS envelope of the riboswitch-$tRNA_2^{Gly,gcc}$ complex suggests that tRNA contacts the T-box riboswitch core at two sites, the proximal region of stem I and the anti-terminator stem (Figure 3C). Thus, both of the Specifier codon-anticodon and acceptor stem-antiterminator loop interactions appear to form when stem I and the antiterminator stem are presented to tRNA.

The orientation of the bound tRNA was intriguing in light of crystal structures of tRNA-stem I complexes derived from *O. iheyensis* and *Geobacillus kaustophilus glyQS* T-box riboswitches [13, 16].

These crystal structures show that in the absence of the stem III and antiterminator stem, the tRNA elbow stacks against a platform composed of a network of base-base interactions between the AG box and apical loop. Because of the apparent role of the platform in the binding of tRNA to stem I, this region of the *B. subtilis* stem I was examined to assess its roles in the structural organization. The

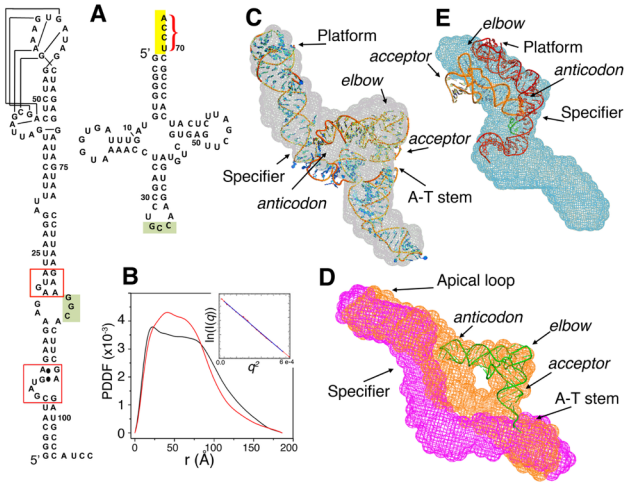

Figure 3. SAXS analysis of the T-box riboswitch core in complex with tRNA. Secondary structures of (A) stem I of the *glyQ* mRNA leader T-box riboswitch derived from *O.iheyensis* and $tRNA^{Gly}$. Nucleotides of the conserved loop E motif in the Specifier domain are boxed (red). The *O. iheyensis* stem I was used to examine possible differential effects on tRNA binding originating from the stem I sequence. In addition to full length $tRNA^{Gly}$, a construct lacking the four unpaired nucleotides highlighted in yellow at the 3' end, $tRNA^{Gly\text{-}4}$, was designed to prevent pairing between the acceptor stem and the T-box loop, mimicking the aminoacylated state of tRNA. (B) Pair distance distribution function plots of the riboswitch core alone (black) and riboswitch core-tRNA complex (red). Guinier region of scattering curve indicates complex is monodisperse (inset). (C) Molecular envelopes of the riboswitch core-tRNA complex derived in 3mM Mg^{2+} (green) overlain on the riboswitch core molecular envelope (gray). (D) Overlay of molecular envelopes of the stem I insertion variant free (pink) and in complex with $tRNA_2^{Gly,gcc}$ (orange). tRNA binds the stem I variant, which cannot form the platform created by apical loop and AG box interactions, in the same conformation as the native sequence. (E) SAXS model of *B. subtilis* riboswitch core in complex with the 3'-truncated tRNA, $tRNA^{Gly\text{-}4}$. Binding involves the anticodon and Specifier domain and the elbow-platform interactions. Atomic model was based on coordinates for crystal structure 4lck [13].

imino NMR spectrum (Figure 4) confirms the predicted secondary structure of the sequence and reveals the presence of the intra-apical loop reverse-Hoogsteen A-U base pair found in the platforms of *O. iheyensis* and *G. kaustophilus*. The spectrum indicates the distal region of the *B. subtilis* stem I is well-ordered and maintains a pattern of inter-loop base-base interactions consistent with the platform. Finally, the effect of Mg^{2+} on the overall fold of the riboswitch core and accommodation of tRNA within the core was examined. Increasing the concentration from 3 mM to 17 mM Mg^{2+} leads to slight compaction of the riboswitch and complex molecular envelopes, but does not change their basic shape (Figure 1F,G and S6).

To determine if the tRNA-riboswitch complex is able to form in the absence of the platform structure, the i-stem I riboswitch variant was mixed with tRNA and examined by SAXS. The insertion of the 18 base pair helix displaces the apical loop from the AG box >50Å and prevents formation of the platform. The SAXS data show the tRNA and i-stem I form a homogeneous complex (Figure 3D) with a comformation that mirrors the tRNA-riboswitch core complex (Figure 3C).

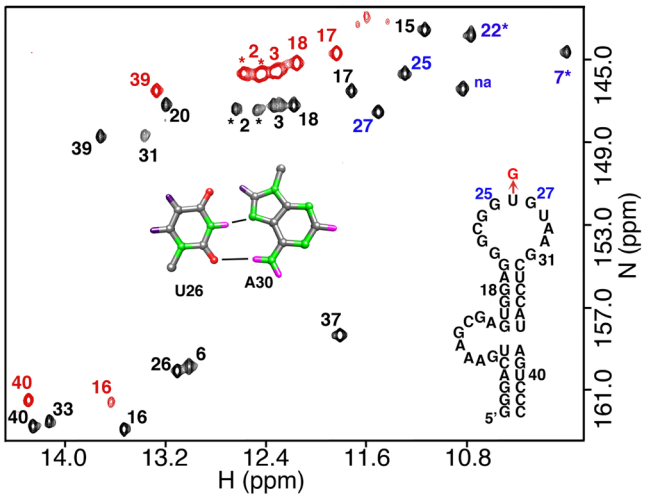

Figure 4. Secondary structure of double T loop molecule used to model the distal end of stem I of the *glyQS* T-box riboswitch. The imino regions of ^{15}N-^{1}H HSQC spectra are shown for the native (black) and U70G mutant (red) sequences. Red peaks have been shifted upfield 2.0 ppm in ^{15}N for clarity. Substitution of U with G precludes the intraloop reverse Hoogsteen U-A base pair and leads to loss of most upfield resonances indicative of the folded tertiary structure.

The complex presented above is designed to mimic the transcription read-through state of the T-box riboswitch in complex with uncharged tRNA. Interestingly, the elbow of the tRNA molecule does not contact the platform of stem I when the T-box loop is present. To confirm that the platform-elbow interaction can exist in the context of the core riboswitch, a $tRNA_2^{Gly,gcc}$ molecule that lacks the four single strand nucleotides at the 3' end ($tRNA^{Gly-4}$) was prepared (Figure 3A). This deletion prevents the tRNA molecule from pairing with the T-box loop but does not alter the ability of tRNA to form the anticodon-Specifier codon and tRNA elbow-platform interactions. SAXS data for the $tRNA^{Gly-4}$–riboswitch core complex show that the tRNA binds the Specifier and platform elements of the riboswitch (Figure 3E). This bound conformation is supported by ribonuclease T1 and V1 protection and Fe-EDTA hydroxyl radical cleavage experiments of tRNA in complex with either the T-box riboswitch core or the stem I only RNA construct (Figure S3). tRNA bound to stem I only has enhanced hydroxyl radical reactivity of C59 at the loop-helix junction of the T-arm relative to free and riboswitch-

bound tRNA. In addition, nucleotides G18 and G55 in the D- and T-loops, respectively, of tRNA are partially susceptible to T1 cleavage in complex with stem I, but exhibit enhanced cleavage in free tRNA and the riboswitch core complex (Figure S3). Importantly, G33 in the anticodon loop which pairs with the Specifier domain is equally protected from T1 cleavage in both the stem I only and the riboswitch core complexes. The V1 cleavage pattern in the acceptor stem of tRNA bound to the riboswitch core shows protection relative to free or stem 1-bound tRNA, consistent with steric interference of the enzyme by from the T-box loop:acceptor stem intermolecular interaction. No significant RNase V1 differences are observed for the D- and T-loop nucleotides among the three tRNA forms. The similarity of free tRNA and tRNA:riboswitch core complex RNase T1 and hydroxyl radical cleavage patterns at nucleotides that contribute to the tRNA elbow is consistent with the absence of the platform:elbow interaction in the riboswitch core:tRNA complex at equilibrium. The binding mode of $tRNA^{Gly\text{-}4}$ suggests formation of the acceptor stem-antiterminator stem interaction leads to the release of the $tRNA^{Gly}$ elbow from the platform and results in the binding orientation observed at equilibrium in the native complex.

To examine possible sequence-specific contributions of stem I on tRNA binding, SAXS profiles were examined for complexes of $tRNA_2^{Gly,gcc}$ and molecules containing the stem I nucleotide corresponding to the *O. iheyensis* glycyl T-box riboswitch. Complexes formed between $tRNA_2^{Gly,gcc}$ and helices corresponding to the stem I sequences of *B. subtilis* and *O. iheyensis* riboswitches are very similar and clearly exhibit the Specifier-anticodon and platform-elbow interactions (Figure S4). Similarly, substitution of the *O. iheyensis* stem I sequence into the core riboswitch molecule yields a SAXS envelope nearly identical to that of the native *B. subtilis* stem I sequence (Figure S5) and indicates that the general three-dimensional structure is preserved. However, SAXS experiments performed using the complex of $tRNA_2^{Gly,gcc}$ and the *O. iheyensis* stem I-substituted core riboswitch suggest sequence identity may contribute differentially to complex dynamics. The Guinier region of the scattering profile of this complex is not linear, implying possible conformational inhomogeneity. Since the same tRNA sequence was used for the *O. iheyensis* and *B. subtilis* complexes, differences in the dynamics of the complexes are conferred through stem I.

Characterization of T-box RNA and complexes with tRNA using size exclusion FPLC chromatography

Size exclusion chromatography was used to follow complex formation and to the relative compactness of RNAs and complexes using $tRNA_2^{Gly,gcc}$, $tRNA^{Gly-4}$, and the riboswitch core molecules containing stem I sequences corresponding to *B. subtilis glyQS* (Figure 1A) and *O. iheyensis glyQ* (Figure 3A) genes. The *B. subtilis* riboswitch core molecule elutes with a peak centered at 15.6 ml and has a small shoulder at 18.5 ml (Figure 5A) whereas the riboswitch core containing the *O. iheyensis* stem I

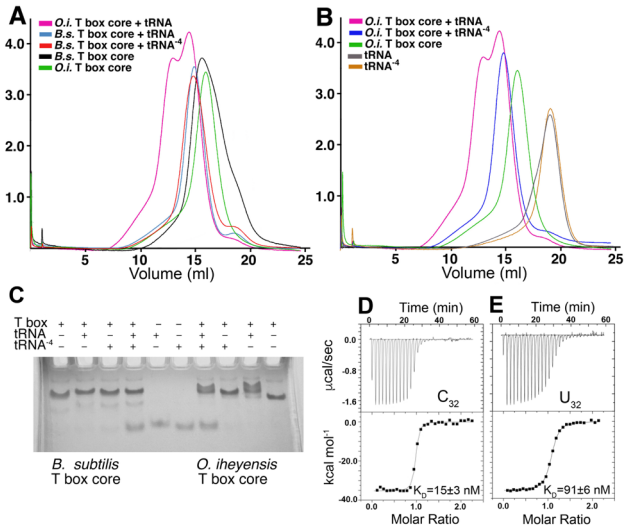

Figure 5. Size exclusion chromatography exclusion profiles of T-box riboswitch core molecules and T-box core-tRNA complexes. Chromatography was performed at 4 °C using a Superdex 200 (10/300). (A) The apparent minor heterogeneity exhibited by the riboswitch core composed of stem 1 corresponding to *B. subtilis glyQS* mRNA leader disappears upon binding of $tRNA^{Gly}$ and $tRNA^{Gly-4}$. Interestingly, complexes with both tRNAs have similar retention volumes. However, the riboswitch core composed of stem 1 corresponding to *O. iheyensis glyQ* mRNA leader adopts two distinctly different global conformations when bound to tRNA with the slower running complex eluting similar to the *B. subtilis* riboswitch core complexes. (B) The *O. iheyensis* riboswitch core binds $tRNA^{Gly-4}$ (which cannot pair with the T-box loop) and forms a complex with a retention time similar to the slower running species formed between the riboswitch core and full length tRNA. (C) Native gel migration patterns of *B. subtilis* and *O. iheyensis* stem I riboswitch core molecules and their tRNA complexes. In lanes 4 and 7, the ratio $tRNA^{Gly-4}$:$tRNA^{Gly}$:riboswitch ratio is 1:1:1. The migration patterns are consistent with the SEC profiles. The *B. subtilis* stem I T-box forms a complex with the truncated tRNA (lane 3), but preferentially binds full length tRNA (lanes 4-6). The T-box riboswitch with *O. iheyensis* stem I sequence also appears to preferentially select full length tRNA (lanes 5-7), but the bound state with full length tRNA is heterogeneous (lane 9). ITC thermograms of the *B. subtilis* riboswitch stem I with (D) $tRNA_2^{Gly,gcc}$ and (E) $C_{32}U$ $tRNA_2^{Gly,gcc}$.

sequence elutes as a sharper peak at 15.9 ml (Figure 5B). As expected, the $tRNA_2^{Gly,gcc}$ and $tRNA^{Gly-4}$ molecules are retained longest and elute as single peaks (peak maxima at 18.6 and 18.9 ml, respectively) (Figure 5B).

The elution profiles of riboswitch-tRNA complexes were examined next. The *B. subtilis* stem I

riboswitch core molecule in complex with either $tRNA_2^{Gly,gcc}$ or $tRNA^{Gly-4}$ elutes as a single sharp peak with retention volume maxima at 15.0 ml and 14.9 ml, respectively (Figure 5A). Although, the rate of migration through the resin is a combination of molecular size and overall compactness, molecules that exhibit the same retention time need not have the same shape. Both $tRNA_2^{Gly,gcc}$ and $tRNA^{Gly-4}$ can form complexes with the riboswitch that include the tRNA elbow-double T-loop interaction and the anticodon-Specifier codon interaction, but only $tRNA_2^{Gly,gcc}$ can also form the acceptor stem-T-box antiterminator loop intermolecular helix. These elution profiles appear consistent with the SAXS data which indicate somewhat extended conformations of the complexes relative to the more compact conformation expected when the tRNA binds the riboswitch platform and Specifier and antiterminator loop nucleotides at the same time. The elution profiles of the *O. iheyensis* stem I riboswitch core molecule in complex with $tRNA_2^{Gly,gcc}$ and $tRNA^{Gly-4}$ are particularly informative. The complex with $tRNA_2^{Gly,gcc}$ elutes as two peaks (12.8 ml and 14.6 ml) with ~15% greater population of molecules in the slower migrating peak (Figure 5B). Increasing the mole ratio of tRNA to riboswitch from 1:1 to 3:1 causes slight broadening of the elution profile for the complex and the appearance of a peak corresponding to the excess unbound tRNA (18.6 ml). However, the complex with $tRNA^{Gly-4}$ elutes as a single sharp peak at 14.7 ml (Figure 5B). As with the *B. subtilis* riboswitch core molecule, only the anticodon-Specifier codon and tRNA elbow-double T-loop interactions are possible in the complex with $tRNA^{Gly-4}$ (Figure 5A). These elution profiles indicate the *O. iheyensis* riboswitch core molecule in complex with $tRNA_2^{Gly,gcc}$ adopts a second, faster migrating architecture than that of the stem I-tRNA interactions alone. The adoption of two shapes by the *O. iheyensis* stem I-tRNA complex also is consistent with SAXS data that indicate the inhomogeneous nature of the complex.

To explore the possibility that the contrasting solution behavior of the riboswitch-tRNA complexes is rooted in the affinities of *B. subtilis* and *O. iheyensis* stem I for $tRNA^{Gly}$, a series of isothermal titration calorimetry (ITC) measurements were performed. The affinities of the tRNA-stem I interactions are very similar, K_d = 15±3 nM and 21±2.4 nM for *B. subtilis* and *O. iheyensis*, respectively (Figure 5D). These affinities are 7-8 fold tighter than previously reported for the *O. iheyensis* stem I and $tRNA_3^{Gly}$ [13]. The native sequence of $tRNA_3^{Gly}$ (anticodon 5'-GCC-3') contains a U_{32}-A_{38} pair which

could lead to reduced tRNA-stem I affinity [30, 31]. To test this possibility, ITC measurements were performed using a U32-modified $tRNA_2^{Gly,gcc}$. The resulting tRNA-stem I affinities of K_d = 91±8 nM and 106±14 nM for *B. subtilis* and *O. iheyensis* stems, respectively (Figure 5D), closely agree with affinities reported for the *O. iheyensis* riboswitch [13]. Therefore, the distinct solution behaviors exhibited by the riboswitch-$tRNA^{Gly}$ complexes is not correlated with the affinities of $tRNA^{Gly}$ for *B. subtilis* and *O. iheyensis* stem I molecules, suggesting that variations in secondary structure features of stem I might alter the orientation, and thus interaction, of the tRNA acceptor stem relative to the T-box loop.

Analysis of local platform interactions by NMR

A loss-of-function point mutation, U70G, in the distal loop of stem I of the *tyrS* T-box riboswitch supports a functional role for the platform. This mutation dramatically lowers the basal level of *tyrS* gene expression and causes loss of transcriptional induction under amino acid limiting conditions, consistent with an inability to stabilize the anti-terminator helix [10]. The U70 nucleotide in the apical loop participates in a conserved reverse-Hoogsteen U-A pair and is one member of a base triple interaction that ties together the apical loop and AG box. To examine the impact of the U70G mutation on the structural integrity of the platform, the imino NMR spectra of RNA molecules corresponding to native and mutant sequences were compared (Figure 4). The substitution of U70 with G70 eliminates the reverse-Hoogsteen U-A pair cross peak as well as most of the peaks indicative of tertiary interactions consistent with the platform structure (Figure 4). Notably, when the AG box and apical loop nucleotide sequences are embedded into separate RNA molecules and mixed, only peaks corresponding to the individual molecules are observed in the imino spectrum (Figure S7). Also lost in the G70 mutant spectrum are peaks corresponding to stem nucleotides that flank the AG box: U6, G15, and U37. The G15 and U37 peaks are present, but less intense, in an RNA hairpin that models the upper stem I in which the terminal loop was replaced by a 5'-UUCG-3' tetraloop (Figure S7). Interestingly, the peak for U6 of the U-A pair that flanks the 3' side of the AG box is not present in the spectrum of the model hairpin and is only observed in the context of the intact platform sequence (Figures 4 and S7).

DISCUSSION

One of the most intriguing results revealed by this study is the orientation of tRNA bound to the

riboswitch that models the transcriptional activation state. The contacts between tRNA and the riboswitch localize to regions of intermolecular secondary structure, the Specifier and T-box antiterminator loop sequences of the riboswitch and the anticodon and acceptor stem of tRNA, respectively. This conformation contrasts the binding of tRNA to stem I alone (Figure S4) [13, 16] which involves base pairing between the Specifier sequence and the tRNA anticodon and stacking of the tRNA elbow against a platform at the distal end of stem I. Importantly, the co-crystal structure of the stem I-tRNA complex could not be fitted into the SAXS envelope of the riboswitch core-tRNA complex (Figure S6). The platform is created by the inter-digitation of two T-loop motifs and is composed of multiple base-base interactions formed between nucleotides of the apical loop and the proximally positioned AG box. The double T-loop motif also is present in the L1 stalk of 23S rRNA and in bacterial RNase P where it again functions as a recognition platform for the tRNA elbow [32-34]. In the functioning of the T box, the combination of pairing and stacking interactions between tRNA and stem I has been suggested to serve as a molecular ruler that facilitates structural selection of cognate tRNA during transcription and translation [12, 13, 33].

The U70G loss-of-function mutation in the *tyrS* T-box riboswitch originally highlighted the functional importance of the apical loop [10]. The NMR data indicate this mutation impairs the ability of the platform to properly or stably fold (Figure 4), suggesting the U70G mutation results in an unstable or dynamic platform *in vivo*. Nonetheless, the insertion of an 18 base pair helix between the apical loop and the AG box precludes formation of the platform but does not prevent formation of the tRNA-riboswitch complex (Figure 3D), consistent with our proposed model and domain assignments. Thus, the integrity of the double T loop motif is important for gene expression, but the absence of this motif does not block the ability of tRNA to bind the T-box riboswitch when the antiterminator helix is present and not in competition with the terminator helix, a conformation expected to permit transcriptional read-through. The SAXS-derived conformation of the complex indicates the elbow:platform interaction necessary for capture of the tRNA may release once the acceptor stem and T-box loop nucleotides pair and prevent destabilization of the transcribing RNA polymerase complex.

The SEC and SAXS results combine to offer a more complete picture of the complex and its dynamics. The *B. subtilis* riboswitch accommodates $tRNA^{Gly}$ through anticodon and acceptor stem pairing and $tRNA^{Gly\text{-}4}$ through anticodon pairing and elbow-platform stacking, but the overall architectures of the complexes lead to nearly identical retention times through the SEC column (Figure 5A). The *O. iheyensis* riboswitch binds $tRNA_2^{Gly,gcc}$ and forms two species with different retention times on the SEC column, the slower complex corresponding to anticodon and acceptor stem pairing with the riboswitch. The faster running complex has an architecture that may correspond to anticodon and acceptor stem pairing between the riboswitch and $tRNA_2^{Gly,gcc}$ concurrent with elbow and platform stacking. These results are consistent with native gel (Figure 5C) and SAXS experiments for the riboswitch-$tRNA_2^{Gly,gcc}$ complex that indicate conformational inhomogeneity within the sample.

It has long been established that nucleotides adjacent to the tRNA anticodon, including residues 32 and 38, can influence codon recognition and translation [31, 35, 36]. These residues exhibit anticodon-dependent sequence conservation (28, 34) with the combinations U_{32}-A_{38} and C_{32}-A_{38} highly conserved in $tRNA_3^{Gly}$ and $tRNA_2^{Gly}$ ($tRNA^{Gly}$ with anticodon 5'-UCC-3'), respectively [37]. In the context of the U_{32}-A_{38} base pair, $tRNA_3^{Gly}$ and $tRNA_1^{Gly}$ (anticodon 5'-CCC-3') exhibit discrimination among the glycine codons according to the wobble rules [38, 39]. However, the presence of C_{32} causes loss of third-codon position discrimination and acquisition of the ability of each of the tRNAs to read all four glycine codons [38, 39]. These translational effects correlate with the affinity of tRNA for the ribosomal A-site [31, 35]. The U32C substitution increases the affinity of $tRNA_1^{Gly}$ for the ribosomal A-site by decreasing the off-rate [31] without affecting the association rate. However, the mechanism of complex stabilization may be different for the T-box-tRNA interaction. Binding of tRNA to the A-site involves an EF-Tu-tRNA complex which would not be expected to affect the T-box riboswitch stem I-tRNA interaction. Solution structure studies of glycyl and non-glycyl anticodon arms demonstrate that the U_{32}-A_{38} nucleotide combination extends the helix by two base pairs, resulting in a tri-loop of residues 34, 35, and 36 rather than the archetypal seven-nucleotide loop [40, 41]. A similar tri-loop is observed for the C_{32}-A_{38} combination in variously modified forms of *Escherichia coli* $tRNA^{Lys}$ anticodon arm [42]. The U32C substitution in $tRNA_3^{Gly}$ prevents formation of base pairs U_{32}-A_{38} and U_{33}-A_{37} and creates the seven-nucleotide

anticodon loop in the uncomplexed anticodon arm [43]. Thus, the enhanced T-box-tRNA affinity conferred by the C_{32}-A_{38} combination in the context of anticodon GCC could result from lowering the barrier to anticodon-Specifier codon pairing by opening up the anticodon loop and increasing the rate of association. The $tRNA_2^{Gly,gcc}$ might be expected to enhance the anti-termination function of the T-box riboswitch relative to the lower affinity the U_{32} $tRNA_2^{Gly,gcc}$ variant. Indeed, a U32C substitution when combined with base pair substitutions in the acceptor stem of *B. subtilis* $tRNA^{Ala}$ enhances transcription read-through of the *Clostridium acetobutylicum alaS* T-box riboswitch at low tRNA concentrations [44].

Our results now allow us to extend the model (Figure 6) for T-box riboswitch function where

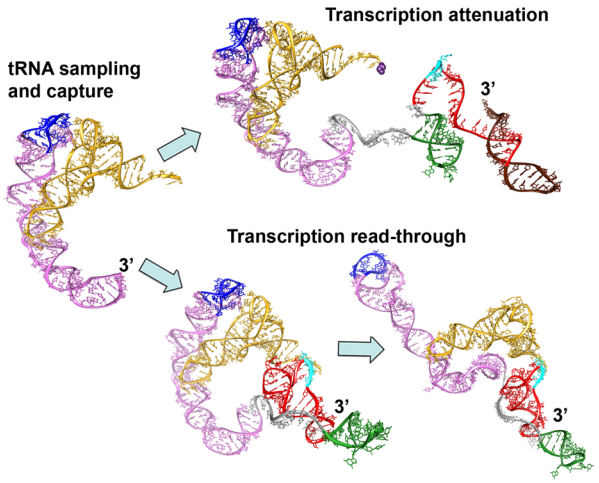

Figure 6. Scheme illustrating a proposed "capture and release" model for formation of the T-box riboswitch-tRNA complex. Collectively, the stem I-tRNA co-crystal structures and the SAXS models of tRNA-riboswitch core complexes support a binding mechanism in which the tRNA is captured by stem I and held in position until the T-box loop-acceptor stem intermolecular helix forms, followed by, or in concert with, release of the tRNA elbow. The nucleotides of the complex are colored as follows: tRNA (gold), stem I (pink), apical loop (blue), single strand linker (silver), stem III (green), antiterminator stem (red), terminator stem (brown), and antiterminator loop (cyan). The upper diagram shows the glycine (purple surface rendering) aminoacylated form of the tRNA.

tRNA is captured by stem I of the nascent riboswitch transcript to form a meta-stable complex [17, 45]. The acceptor stem of uncharged tRNA can then pair with the T-box loop of the anti-terminator helix, further stabilizing the tRNA-riboswitch complex and suppressing formation of the terminator helix. Thus, the platform-elbow interaction extends the temporal window of opportunity for an uncharged tRNA to prevent attenuation of transcription by increasing the residence time of tRNA as the nascent riboswitch is elongated 3' to form the antiterminator and/or terminator helices. As the RNA sequence

corresponding to the anti-terminator helix exits the transcription machinery and folds, the 3' end of the bound tRNA is available for the tRNA aminoacylation state to be interrogated. Our modeling suggests that the anti-terminator stem and stem III form an extended coaxially stacked helix. In this extended "capture-and-release" model for T-box function (Figure 6), we speculate that formation of the T-box loop-acceptor stem intermolecular pairing will lead to stacking or other conformational changes that cause the tRNA elbow to be displaced from the double T loop, resulting in the global conformation of the complex reflected by the SAXS envelope. This model is consistent with genetic studies that show a tRNA with an acceptor stem extended by one helical turn promotes transcription read-through as effectively as native tRNA [46]. In this case, the Specifier codon-anticodon interaction may allow the tRNA to pivot so that the acceptor stem:antiterminator loop interaction and helical stacking can be maintained even though the distance between the elbow and 3' end of tRNA is increased by ~35 Å.

ACKNOWLEDGEMENT

We thank the W. M. Keck Foundation and the John S. Dunn Foundation for support of the 800 MHz NMR spectrometer. Use of the shared scattering beamline 12-ID-B resource is allocated under the PUP-24152 agreement between the National Cancer Institute and Argonne National Laboratory (ANL). We thank Dr. Lixin Fan (NCI), and Dr. Xiaobing Zuo (ANL) for their expert support.

SUPPORTING INFORMATION

Additional methodological details, Table of SAXS-derived structural parameters, Figures of SAXS envelopes of T-box constructs and ribonuclease cleavage experiments

FUNDING

This work was supported by National Institutes of Health grant GM115857 to E.P.N., grants from the China Youth 1000-Talent Program of the State Council of China, the Beijing Advanced Innovation Center for Structural Biology, the Tsinghua-Peking Joint Center for Life Sciences to XY.F., and the NIH Intramural Research Fund to Y-X.W.

REFERENCES

[1] Henkin, T. M. (2000) Transcription termination control in bacteria, *Curr. Opin. Microbiol. 3*, 149-153.

[2] Henkin, T. M. (2008) Riboswitch RNAs: using RNA to sense cellular metabolism, *Genes Dev. 22*, 3383-3390.

[3] Henkin, T. M. (1994) tRNA-directed transcription antitermination, *Mol. Microbiol. 13*, 381-387.

[4] Zhang, J., and Ferre-D'Amare, A. R. (2015) Structure and mechanism of the T-box riboswitches, *Wiley Interdiscip. Rev.: RNA 6*, 419-433.

[5] Grundy, F. J., Rollins, S. M., and Henkin, T. M. (1994) Interaction between the acceptor end of tRNA and the T box stimulates antitermination in the *Bacillus subtilis tyrS* gene: a new role for the discriminator base, *J. Bacteriol. 176*, 4518-4526.

[6] Vitreschak, A. G., Mironov, A. A., Lyubetsky, V. A., and Gelfand, M. S. (2008) Comparative genomic analysis of T-box regulatory systems in bacteria, *RNS 14*, 717-735.

[7] Wels, M., Groot Kormelink, T., Kleerebezem, M., Siezen, R. J., and Francke, C. (2008) An *in silico* analysis of T-box regulated genes and T-box evolution in prokaryotes, with emphasis on prediction of substrate specificity of transporters, *BMC Genomics 9*, 330.

[8] Winkler, W. C., Grundy, F. J., Murphy, B. A., and Henkin, T. M. (2001) The GA motif: an RNA element common to bacterial antitermination systems, rRNA, and eukaryotic RNAs, *RNA 7*, 1165-1172.

[9] Caserta, E., Liu, L. C., Grundy, F. J., and Henkin, T. M. (2015) Codon-Anticodon Recognition in the *Bacillus subtilis glyQS* T Box Riboswitch: RNA-dependent codon selection outside the ribosome, *J. Biol. Chem. 290*, 23336-23347.

[10] Rollins, S. M., Grundy, F. J., and Henkin, T. M. (1997) Analysis of cis-acting sequence and structural elements required for antitermination of the *Bacillus subtilis tyrS* gene, *Mol. Microbiol. 25*, 411-421.

[11] Wang, J., Henkin, T. M., and Nikonowicz, E. P. (2010) NMR structure and dynamics of the Specifier Loop domain from the *Bacillus subtilis tyrS* T box leader RNA, *Nucleic Acids Res. 38*,

3388-3398.

[12] Grigg, J. C., Chen, Y., Grundy, F. J., Henkin, T. M., Pollack, L., and Ke, A. (2013) T box RNA decodes both the information content and geometry of tRNA to affect gene expression, *Proc. Natl. Acad. Sci. U S A 110*, 7240-7245.

[13] Zhang, J., and Ferre-D'Amare, A. R. (2013) Co-crystal structure of a T-box riboswitch stem I domain in complex with its cognate tRNA, *Nature 500*, 363-366.

[14] Gerdeman, M. S., Henkin, T. M., and Hines, J. V. (2003) Solution structure of the *Bacillus subtilis* T-box antiterminator RNA: seven nucleotide bulge characterized by stacking and flexibility, *J. Mol. Biol. 326*, 189-201.

[15] Wang, J., and Nikonowicz, E. P. (2011) Solution structure of the K-turn and Specifier Loop domains from the *Bacillus subtilis tyrS* T-box leader RNA, *J Mol Biol 408*, 99-117.

[16] Grigg, J. C., and Ke, A. (2013) Structural determinants for geometry and information decoding of tRNA by T box leader RNA, *Structure 21*, 2025-2032.

[17] Grundy, F. J., Yousef, M. R., and Henkin, T. M. (2005) Monitoring uncharged tRNA during transcription of the *Bacillus subtilis glyQS* gene, *J. Mol. Biol. 346*, 73-81.

[18] Nikonowicz, E. P., Sirr, A., Legault, P., Jucker, F. M., Baer, L. M., and Pardi, A. (1992) Preparation of ^{13}C and ^{15}N labelled RNAs for heteronuclear multi-dimensional NMR studies, *Nucleic Acids Res. 20*, 4507-4513.

[19] Svergun, D. I. (1999) Restoring low resolution structure of biological macromolecules from solution scattering using simulated annealing, *Biophys. J. 76*, 2879-2886.

[20] Volkov, V. V., and Svergun, D. I. (2003) Uniqueness of *ab initio* shape determination in small-angle scattering, *J. Appl. Crystallogr. 36*, 860-864.

[21] Kozin, M. B., and Svergun, D. I. (2001) Automated matching of high- and low-resolution structural models, *J. Appl. Crystallogr. 34*, 33-41.

[22] Grundy, F. J., Winkler, W. C., and Henkin, T. M. (2002) tRNA-mediated transcription antitermination in vitro: codon-anticodon pairing independent of the ribosome, *Proc. Natl. Acad. Sci. U S A 99*, 11121-11126.

[23] Yousef, M. R., Grundy, F. J., and Henkin, T. M. (2005) Structural transitions induced by the interaction between $tRNA^{Gly}$ and the *Bacillus subtilis glyQS* T box leader RNA, *J. Mol. Biol. 349*, 273-287.

[24] Rambo, R. P., and Tainer, J. A. (2015) Modeling macromolecular motions by x-ray-scattering-constrained molecular dynamics, *Biophys. J. 108*, 2421-2423.

[25] Petoukhov, M. V., Franke, D., Shkumatov, A. V., Tria, G., Kikhney, A. G., Gajda, M., Gorba, C., Mertens, H. D., Konarev, P. V., and Svergun, D. I. (2012) New developments in the program package for small-angle scattering data analysis, *J .Appl. Crystallogr. 45*, 342-350.

[26] Fang, X., Wang, J., O'Carroll, I. P., Mitchell, M., Zuo, X., Wang, Y., Yu, P., Liu, Y., Rausch, J. W., Dyba, M. A., Kjems, J., Schwieters, C. D., Seifert, S., Winans, R. E., Watts, N. R., Stahl, S. J., Wingfield, P. T., Byrd, R. A., Le Grice, S. F., Rein, A., and Wang, Y. X. (2013) An unusual topological structure of the HIV-1 Rev response element, *Cell 155*, 594-605.

[27] Lipfert, J., Herschlag, D., and Doniach, S. (2009) Riboswitch conformations revealed by small-angle X-ray scattering, *Methods Mol. Biol. 540*, 141-159.

[28] Rambo, R. P., and Tainer, J. A. (2010) Improving small-angle X-ray scattering data for structural analyses of the RNA world, *RNA 16*, 638-646.

[29] Reyes, F. E., Schwartz, C. R., Tainer, J. A., and Rambo, R. P. (2014) Methods for using new conceptual tools and parameters to assess RNA structure by small-angle X-ray scattering, *Methods Enzymol. 549*, 235-263.

[30] Chang, A. T., and Nikonowicz, E. P. (2013) Solution NMR determination of hydrogen bonding and base pairing between the *glyQS* T box riboswitch Specifier domain and the anticodon loop of $tRNA^{Gly}$, *FEBS Lett. 587*, 3495-3499.

[31] Olejniczak, M., and Uhlenbeck, O. C. (2006) tRNA residues that have coevolved with their anticodon to ensure uniform and accurate codon recognition, *Biochimie 88*, 943-950.

[32] Korostelev, A., Trakhanov, S., Laurberg, M., and Noller, H. F. (2006) Crystal structure of a 70S ribosome-tRNA complex reveals functional interactions and rearrangements, *Cell 126*, 1065-1077.

[33] Lehmann, J., Jossinet, F., and Gautheret, D. (2013) A universal RNA structural motif docking the elbow of tRNA in the ribosome, RNAse P and T-box leaders, *Nucleic Acids Res. 41*, 5494-5502.

[34] Reiter, N. J., Osterman, A., Torres-Larios, A., Swinger, K. K., Pan, T., and Mondragon, A. (2010) Structure of a bacterial ribonuclease P holoenzyme in complex with tRNA, *Nature 468*, 784-789.

[35] Olejniczak, M., Dale, T., Fahlman, R. P., and Uhlenbeck, O. C. (2005) Idiosyncratic tuning of tRNAs to achieve uniform ribosome binding, *Nat. Struct. Mol. Biol. 12*, 788-793.

[36] Yarus, M. (1982) Translational efficiency of transfer RNA's: uses of an extended anticodon, *Science, 218*, 646-652.

[37] Chan, P. P., and Lowe, T. M. (2009) GtRNAdb: a database of transfer RNA genes detected in genomic sequence, *Nucleic Acids Res. 37*, D93-97.

[38] Claesson, C., Lustig, F., Boren, T., Simonsson, C., Barciszewska, M., and Lagerkvist, U. (1995) Glycine codon discrimination and the nucleotide in position 32 of the anticodon loop, *J. Mol. Biol. 247*, 191-196.

[39] Lustig, F., Boren, T., Claesson, C., Simonsson, C., Barciszewska, M., and Lagerkvist, U. (1993) The nucleotide in position 32 of the tRNA anticodon loop determines ability of anticodon UCC to discriminate among glycine codons, *Proc. Natl. Acad. Sci. U S A 90*, 3343-3347.

[40] Cabello-Villegas, J., Winkler, M. E., and Nikonowicz, E. P. (2002) Solution conformations of unmodified and A_{37} N^6-dimethylallyl modified anticodon stem-loops of *Escherichia coli* $tRNA^{Phe}$, *J. Mol. Biol. 319*, 1015-1034.

[41] Stuart, J. W., Gdaniec, Z., Guenther, R., Marszalek, M., Sochacka, E., Malkiewicz, A., and Agris, P. F. (2000) Functional anticodon architecture of human $tRNA^{Lys3}$ includes disruption of intraloop hydrogen bonding by the naturally occurring amino acid modification, t^6A, *Biochemistry 39*, 13396-13404.

[42] Durant, P. C., Bajji, A. C., Sundaram, M., Kumar, R. K., and Davis, D. R. (2005) Structural effects of hypermodified nucleosides in the *Escherichia coli* and human $tRNA^{Lys}$ anticodon loop: the

effect of nucleosides s^2U, mcm^5U, mcm^5s^2U, mnm^5s^2U, t^6A, and ms^2t^6A, *Biochemistry 44*, 8078-8089.

[43] Chang, A. T., and Nikonowicz, E. P. (2012) Solution nuclear magnetic resonance analyses of the anticodon arms of proteinogenic and nonproteinogenic $tRNA^{Gly}$, *Biochemistry 51*, 3662-3674.

[44] Liu, L. C., Grundy, F. J., and Henkin, T. M. (2015) Non-conserved residues in *Clostridium acetobutylicum* $tRNA^{Ala}$ contribute to tRNA tuning for efficient antitermination of the *alaS* T Box riboswitch, *Life 5*, 1567-1582.

[45] Nelson, A. R., Henkin, T. M., and Agris, P. F. (2006) tRNA regulation of gene expression: interactions of an mRNA 5'-UTR with a regulatory tRNA, *RNA 12*, 1254-1261.

[46] Yousef, M. R., Grundy, F. J., and Henkin, T. M. (2003) tRNA requirements for *glyQS* antitermination: a new twist on tRNA, *RNA 9*, 1148-1156.